

## Local characterization of collagen architecture and mechanical properties of tissue engineered atherosclerotic plaque cap analogs

Crielaard, Hanneke; Wissing, Tamar B.; Guvenir Torun, Su; Kremers, Gert Jan; de Miguel, Pablo; Hengst, Ranmadusha M.; Gijssen, Frank J.H.; Akyildiz, Ali C.; van der Heiden, Kim

**DOI**

[10.1016/j.actbio.2025.01.035](https://doi.org/10.1016/j.actbio.2025.01.035)

**Publication date**

2025

**Document Version**

Final published version

**Published in**

Acta Biomaterialia

**Citation (APA)**

Crielaard, H., Wissing, T. B., Guvenir Torun, S., Kremers, G. J., de Miguel, P., Hengst, R. M., Gijssen, F. J. H., Akyildiz, A. C., & van der Heiden, K. (2025). Local characterization of collagen architecture and mechanical properties of tissue engineered atherosclerotic plaque cap analogs. *Acta Biomaterialia*, 194, 185-193. <https://doi.org/10.1016/j.actbio.2025.01.035>

**Important note**

To cite this publication, please use the final published version (if applicable).  
Please check the document version above.

**Copyright**

Other than for strictly personal use, it is not permitted to download, forward or distribute the text or part of it, without the consent of the author(s) and/or copyright holder(s), unless the work is under an open content license such as Creative Commons.

**Takedown policy**

Please contact us and provide details if you believe this document breaches copyrights.  
We will remove access to the work immediately and investigate your claim.



Full length article



## Local characterization of collagen architecture and mechanical properties of tissue engineered atherosclerotic plaque cap analogs

Hanneke Crielaard<sup>a</sup>, Tamar B. Wissing<sup>a,b</sup>, Su Guvenir Torun<sup>a</sup>, Gert-Jan Kremers<sup>d</sup>, Pablo de Miguel<sup>a,c</sup>, Ranmadusha M. Hengst<sup>a,c</sup>, Frank J.H. Gijzen<sup>a,c</sup>, Ali C. Akyildiz<sup>a,c,\*</sup>, Kim van der Heiden<sup>a</sup>

<sup>a</sup> Department of Cardiology, Biomedical Engineering, Cardiovascular Institute, Thorax Center, Erasmus MC, Rotterdam, The Netherlands

<sup>b</sup> Department of Biomedical Engineering, Eindhoven University of Technology, Eindhoven, The Netherlands

<sup>c</sup> Department of Biomechanical Engineering, Delft University of Technology, Delft, The Netherlands

<sup>d</sup> Erasmus Optical Imaging Center, Erasmus Medical Center, Rotterdam, The Netherlands

### ARTICLE INFO

#### Keywords:

Atherosclerosis  
Plaque rupture  
Mechanics  
Collagen  
Tissue engineering

### ABSTRACT

Many cardiovascular events are triggered by fibrous cap rupture of an atherosclerotic plaque in arteries. However, cap rupture, including the impact of the cap's structural components, is poorly understood. To obtain better mechanistic insights in a biologically and mechanically controlled environment, we previously developed a tissue-engineered fibrous cap model. In the current study, we characterized the (local) structural and mechanical properties of these tissue-engineered cap analogs. Twenty-four collagenous cap analogs were cultured. The analogs were imaged with multiphoton microscopy with second-harmonic generation to obtain local collagen fiber orientation and dispersion. Then, the analogs were mechanically tested under uniaxial tensile loading until failure, and the local deformation (strain) and failure characteristics were analyzed. Our results demonstrated that the tissue-engineered analogs mimic the dominant (circumferential) fiber direction of human plaques. The analogs also exhibited a physiological strain stiffening response, similar to human fibrous plaque caps. Ruptures in the analogs initiated in and propagated towards local high-strain regions. The local strain values at the rupture sites were similar to the ones reported for carotid human fibrous plaque tissue. Finally, the study revealed that the rupture propagation path in the analogs followed the local fiber direction.

*Statement of significance:* Many cardiovascular events are triggered by mechanical rupture of atherosclerotic plaque caps. Yet, cap rupture mechanics is poorly understood. This is mainly due to the scarcity of plaques for high-throughput testing and the structural complexity of plaques. To overcome this, we previously developed tissue-engineered cap analogs. The current study characterizes (local) structural and mechanical properties of these cap analogs. Our findings show that: (1) cap analogs closely mimic human fibrous caps, including fiber orientation and strain stiffening responses; (2) structural and mechanical properties of cap analogs are associated, which provides critical information for understanding plaque rupture; and (3) cap ruptures commonly start in and propagate towards high-strain areas, indicating the potential use of strain measurements for cap rupture risk assessment.

### 1. Introduction

Many cardiovascular events, such as myocardial infarction and ischemic stroke, are triggered by the rupture of the fibrous cap of an atherosclerotic plaque present in a conduit artery [1]. However, plaque cap rupture risk evaluation is currently not part of the clinical cardiovascular event risk assessment protocol [2]. This is mainly because the

so-far-proposed (mainly geometric) criteria, such as cap thickness [3] and lipid core size [4], fail to provide sufficient predictive power for the complex cap rupture phenomenon [5,6]. From the biomechanics perspective, cap rupture is a material failure of this collagenous plaque structure, where the cap cannot maintain its structural integrity under the loading exerted on it [7]. Hence, biomechanical assessment of atherosclerotic plaques has the potential to provide new insights into

\* Corresponding author at: Department of Biomedical Engineering, Biomechanics Laboratory, Ee2341, P.O. Box 2040, 3000 CA Rotterdam, The Netherlands.

E-mail address: [a.akyildiz@erasmusmc.nl](mailto:a.akyildiz@erasmusmc.nl) (A.C. Akyildiz).

<https://doi.org/10.1016/j.actbio.2025.01.035>

Received 20 September 2024; Received in revised form 13 January 2025; Accepted 21 January 2025

Available online 22 January 2025

1742-7061/© 2025 The Authors. Published by Elsevier Inc. on behalf of Acta Materialia Inc. This is an open access article under the CC BY-NC-ND license (<http://creativecommons.org/licenses/by-nc-nd/4.0/>).

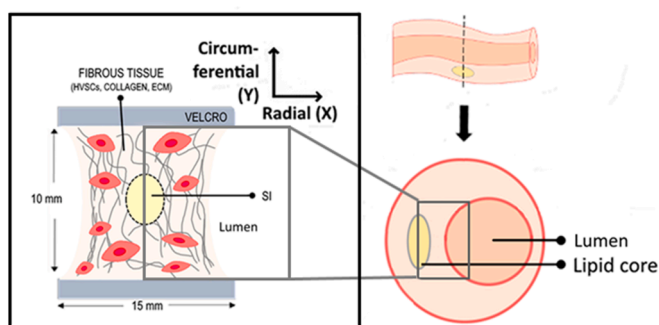
understanding the cap rupture and new markers for improved cap rupture risk assessment.

The mechanical behavior of biological tissues is known to be governed by the tissue’s (micro)structure. In healthy arteries, collagen is one of the main load-bearing components and the mechanical properties of the arteries majorly depend on the properties of the underlying collagen fibers and their organization [8]. The fibrous plaque tissue is also highly collagenous [9–12], yet the impact of the collagenous matrix architecture on the tissue’s mechanical properties, including the material failure characteristics, is not well understood. Only recently, Johnston et al. [12] reported predominant circumferential orientation of the collagen fibers in the majority of carotid plaque caps of carotid endarterectomy (CEA) samples. They also measured higher ultimate stresses and lower ultimate strains for these caps [12]. We also recently showed, utilizing a mechano-imaging experimental protocol we designed [13],

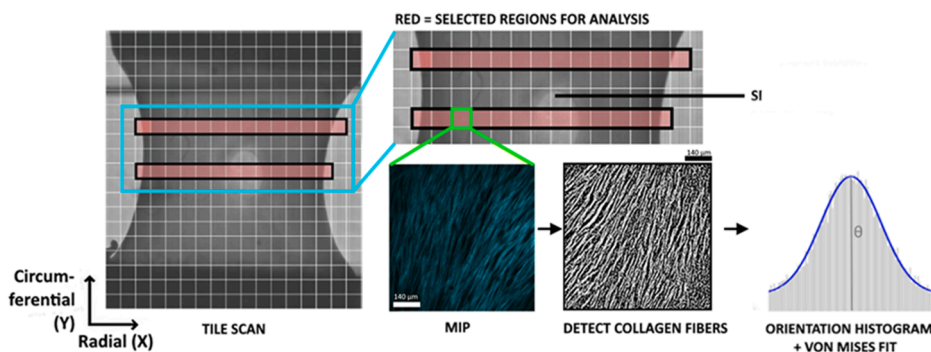
that not only the caps but the entire fibrous plaque tissue from CEA samples had a circumferential orientation predominantly, and also observed unavoidable inter- and intra-plaque variation. Moreover, uniaxial tensile testing of the samples revealed a nonuniform distribution of tensile strain within the specimens and a statistically significantly higher local strain at the rupture initiation site than in the rest of the specimens [10].

An important limiting factor in experimental plaque rupture research is the scarcity of testable human plaque samples, which makes it difficult to perform high-throughput testing. To overcome this shortcoming, we recently developed a collagenous tissue-engineered fibrous cap model [14] as a human disease model. These analogs enable conducting studies with a large enough sample size and varying structural composition. As a first step of this human disease model, we specifically focused on thin cap fibroatheromas (TCFAs)/vulnerable plaques, since these are most

### A. Development of tissue-engineered fibrous cap analogs



### B. Multiphoton microscopy with second-harmonic generation



### C. Uniaxial tensile testing with digital image correlation

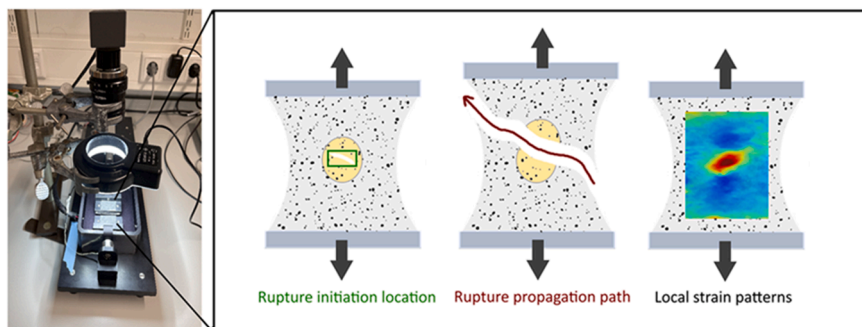


**Fig. 1.** Methodological pipeline of the study. A) Illustration of a tissue-engineered cap analog (left) and of a simplified geometry of an atherosclerotic plaque cap (right) [14]. (HVSCs: human vena saphena cells, ECM: extracellular matrix) B) Collagen imaging with SHG-MPM and fiber orientation analysis. Scale bar = 140 μm C) Uniaxial tensile testing and DIC-derived local deformation measurements (SHG: second-harmonic generation, MPM: multiphoton microscopy, MIP: Maximum intensity projection, DIC: Digital image correlation).

prone to rupture. These plaques are characterized by a soft lipid core embedded in a collagenous fibrous cap. The model consists of collagenous tissue construct with a soft inclusion at the center, which aims to mechanically mimic the fibrous plaque cap next to a soft lipid-rich necrotic core in real plaques (Fig. 1A). In previous study [14], we demonstrated that these analogs possess a collagenous architecture and collagen types comparable to those found in the fibrous caps of human plaques. Consequently, this human disease model has the great potential to provide a platform to study the biomechanics of and the geometric and structural factors involved in plaque rupture mechanics.

In this study, we aim to characterize the structural and mechanical properties of this fibrous cap model, with a specific focus on obtaining detailed insights into local collagen fiber architecture, and into strain distribution, and the initiation and propagation of rupture under tensile loading. This characterization will serve three primary purposes: (1) to compare the (local) mechanical and structural properties of our tissue-engineered analogs with that of human plaque tissue, thereby evaluating the analogs for their accuracy in mimicking human fibrous cap tissue; (2) to evaluate if local strain can be a potential marker for plaque rupture risk assessment and (3) to identify additional correlations between structural and mechanical properties within our analogs that are challenging to observe in human tissue, but are crucial for enhancing our understanding and prediction of atherosclerotic plaque rupture.

## 2. Materials and methods

### 2.1. Tissue-engineering the fibrous cap analogs

Twenty-four cap analogs (Fig. 1A) were cultured following the methodology described previously in detail [14]. Shortly, vascular-derived myofibroblasts (i.e. human vena saphena cells) were harvested from pieces of saphenous vein, left over after coronary bypass surgery, according to the Dutch guidelines for secondary use of materials. Then, these cells were seeded in  $10 \times 15$  mm-sized fibrin gels between two Velcro strips in a Flexcell system (FX-4000T, Flexcell Int, 196 McKeesport, PA). After seeding, the analogs were statically cultured for 7 days. On day 7, a 2 mm diameter soft inclusion (SI) was created by punching a hole in the center of the analogs and filling it with fibrin. This collagen-poor inclusion aims to mechanically mimic the soft necrotic and/or lipid-rich core of real atherosclerotic plaque. The analogs were then kept under the same static condition for 7 more days, after which they were exposed to intermittent straining in the y-direction of the analog (4 % strain at 0.5 Hz for 1 hr + 0 % strain for 3 hrs) for 7 days, to stimulate collagen synthesis and remodeling [15]. On day 21 the culturing was finished, and the analogs were imaged and mechanically tested.

### 2.2. Multiphoton microscopy imaging

On day 21 of the culturing protocol, a subset of analogs ( $n = 10$ ) were randomly selected for multiphoton microscopy (MPM) imaging with second-harmonic generation (SHG). The analogs were attached to a layer of silicon (Sylgard 184, VWR, Germany, 0.5–1 cm thick) by pinning surgical needles through the Velcro's at both sides of the analog to prevent movement of the analogs during MPM imaging, and submerged in phosphate-buffered saline (PBS) at room temperature. An MPM (TCS SP5 Confocal, Leica, Germany) with a Chameleon Ultra multiphoton laser (710–1040 nm) (Coherent, USA) was used to visualize the collagen architecture. First, an overview scan (~5–10 minutes per analog) splitting the analog into tiles (tile size =  $739 \times 739 \mu\text{m}$ ) was made (Fig. 1B) by using the brightfield mode of the microscope. From this tile scan, two horizontal lines of adjacent tiles were selected for further scanning, to limit the scanning time and prevent tissue degradation. The selected tiles overlaid a part of the fibrous tissue of the analog and a part of the soft inclusion (Fig. 1B). For each tile, z-stack imaging in the depth direction was performed (isotropic in-plane

resolution of  $1.4 \mu\text{m}$ ,  $3 \mu\text{m}$  distance between the stacks, ~5–10 min per tile) using a multiphoton laser with an excitation wavelength of 880 nm and a non-descanned detector with a 430–450 nm emission filter. The images were obtained up to a depth of approximately  $150 \mu\text{m}$  (~30 % of the analog's thickness) from the surface that was facing upwards during culturing. MPM required 4 hours of extra handling, but we did not find significant differences in the global mechanics between the imaged samples and the samples that were not imaged (Supplementary Figure S1).

#### 2.2.1. Data processing

Maximum intensity projection (MIP) images were analyzed with the MATLAB-based fiber orientation analysis tool, FOAtool [16] to detect individual collagen fibers and their orientations. Von Mises distributions were fit to the histogram of the detected collagen fiber orientations in every tile (Fig. 1B). The predominant angle ( $\theta$ ) of the collagen fibers and the dispersion parameter  $\kappa$  per tile were assessed, where the former is the mode of the von Mises distribution and the latter is a structural parameter describing the dispersion of the fiber orientations. The difference between the predominant angle of the collagen fibers and the y-axis (loading direction), denoted as  $\Delta\theta$ , was calculated for each tile. More details on how to obtain the dispersion parameter  $\kappa$  from a von Mises fit can be found in [17]. Here it is worth mentioning that the range of  $\kappa$  is  $[0 : 1/3]$ , where at  $\kappa = 0$ , all collagen fibers are aligned in the direction of  $\theta$ , and at  $\kappa = 1/3$ , the fibers are uniformly distributed in all possible angles.

### 2.3. Mechanical testing

All cap analogs ( $n = 24$ ) were mechanically tested. First, the cross-sectional areas of the analogs were measured with high spatial resolution ultrasound (Vevo 3100, FUJIFILM, Visual Sonics Inc., Canada). A 21 MHz central frequency 2-D linear transducer (MX250, axial resolution =  $75 \mu\text{m}$ ) and a stepper motor were used to capture the cross-sectional area of the analog every  $40 \mu\text{m}$  along the y-direction of the analogs in the unloaded state. After geometry measurements, a speckle pattern for digital image correlation (DIC) was applied to the top surface of the analogs by using an airbrush filled with tissue dye (24,113–2, Polysciences Inc., Ott Scientific). Then, the Velcro strips on each side of the analog were placed in the clamps of a custom-designed uniaxial tensile tester. The tensile tester consisted of two clamps (one stationary and one movable) with sandpaper and foam tape to prevent slippage, a 10 N load cell (LCMFD-10N, Omega Engineering, USA), and a linear actuator (EACM2E10AZAK, Oriental Motor, Japan). A torque screwdriver (Garant, Hoffman group, Germany) was used to apply a torque of 10 cNm to tighten the clamps. The analogs were visually inspected before the tests for any pre-existing tissue damage. Then, the analogs were pre-stretched (0.15 N) to remove the slack. Afterward, 10 cycles of pre-conditioning were performed up to 10 % strain, to ensure a repeatable mechanical response of the analogs [18,19]. Finally, the analogs were strained until failure at a speed of 200 %/min, which mimics the *in vivo* physiological straining rate of plaque tissue [18]. These strain and strain rate values (10 % and 200 %) were based on the initial clamp-to-clamp distance measured by the actuator right before the pre-conditioning of the pre-stretched analogs. During testing, the analogs were completely submerged in a heating bath filled with a PBS solution at  $37^\circ\text{C}$ . Above the tensile tester, a 5.3 Megapixels CMOS Camera (PL-D725, Pixelink, USA) and a light source were mounted, which were used to record videos of the analogs at 30 fps during testing. The frames captured in the videos were used for DIC and the analysis of the rupture initiation location and rupture propagation path.

#### 2.3.1. Data processing

DIC analyses of the video recordings of the analogs during mechanical testing were performed with the open-source 2D DIC software Ncorr (version 1.2) [17]. The region of interest (ROI) for DIC was

defined as the area of the analog excluding  $\sim 1$  mm from each clamp. Areas containing air bubbles were excluded from the analysis to prevent artifacts.

Since the analogs had compacted during culturing in the central section, as also reported before [14], they resembled dogbone shapes, with a reduced cross-sectional area in the center region, referred to as ‘reduced-section’, commonly used for stress and strain assessment for uniaxial tensile testing [20]. The reduced section in our tissue-engineered analogs was defined as the region between two lines spanning from the top to the bottom of the soft inclusion.

The global Green-Lagrange strain ( $\epsilon_{yy}$ ) was defined as the average DIC-derived strain in the tensile direction in the reduced section of the analogs. The global engineering stress was derived from the force measurements and initial average cross-sectional area of the reduced section of each analog, obtained from the ultrasound images using Fiji (Image J) [21]. The stiffness of the global stress-strain ratio curves was obtained for every 0.01 strain increment until a strain value of 0.07 (Supplementary Figure S3). This final strain value was chosen as some analogs experienced rupture initiation shortly after this strain level. Linear regression was performed between data points 0.005 below and above these central strain values to obtain the linear slopes as measures for stiffness.

Rupture initiation locations and the rupture propagation path were detected by visual inspection of the camera images. DIC-derived local tensile strains at the rupture initiation location and the average tensile strains within the entire region of interest of the analog were calculated.

#### 2.4. Statistical methods

Statistical analyses were performed using Matlab (Statistics and Machine Learning Toolbox, MathWorks, USA). All data are presented as the mean  $\pm$  standard deviation unless stated otherwise. Shapiro-Wilk tests were used to determine if the data were normally distributed.

To determine whether there were statistically significant differences within the paired data (e.g., strain values at the rupture location versus average strains of the same analogs), The wilcoxon signed-rank test was used for the non-normally distributed data and paired *t*-test for the

normally distributed data. To determine whether there were statistically significant differences between groups of analogs (e.g., samples with clamp rupture versus central rupture), unpaired *t*-tests were performed. A *p*-value  $< 0.05$  was considered significant (visualized as \*  $p < 0.05$ ; \*\*  $p < 0.01$ ; \*\*\*  $p < 0.001$ ). To study the association between variables, linear regression was used. For linear regression, Pearson correlation coefficient (*r*), coefficient of determination ( $R^2$ ), and *p*-value were calculated.

### 3. Results

#### 3.1. Collagen architecture

The plaque cap analogs consisted of a collagenous fibrous tissue with a soft inclusion which was integrated into the tissue, via cell and collagen ingrowth [14]. Although collagen was also found within the soft inclusion, its amount was much less compared to the surrounding fibrous tissue. This slight infiltration of collagen is essential for ensuring that the soft inclusion adheres to the surrounding fibrous cap analog, promoting structural integration. The fiber direction analysis (Fig. 2A) based on the MIP images of the analogs ( $n = 10$ ) showed that the fibers in the analogs are predominantly oriented along the *y*-direction ( $\theta = 88^\circ \pm 13^\circ$ ), where the fibers in the edge regions (defined as the 3 most left and right tiles) were oriented closer to the *y*-direction than the ones in the center of the analogs ( $\Delta\theta$  from the *y*-axis:  $17^\circ \pm 5$  vs.  $36^\circ \pm 8$ ,  $p < 0.01$ ). The overall dispersion ( $\kappa$ ) for the analogs was  $0.26 \pm 0.01$ , where the edge regions showed less fiber dispersion than the central regions ( $0.27 \pm 0.01$  vs.  $0.24 \pm 0.02$ ,  $p < 0.01$ ). The average dispersion and the average difference of the predominant fiber direction with the *y*-direction per analog were statistically significantly correlated (Fig. 2B,  $R = 0.83$ ,  $p < 0.005$ ).

#### 3.2. Material behavior

Of the 24 analogs, four (two of which underwent SHG-MPM imaging) were excluded from subsequent analyses due to the presence of small ruptures before mechanical testing.

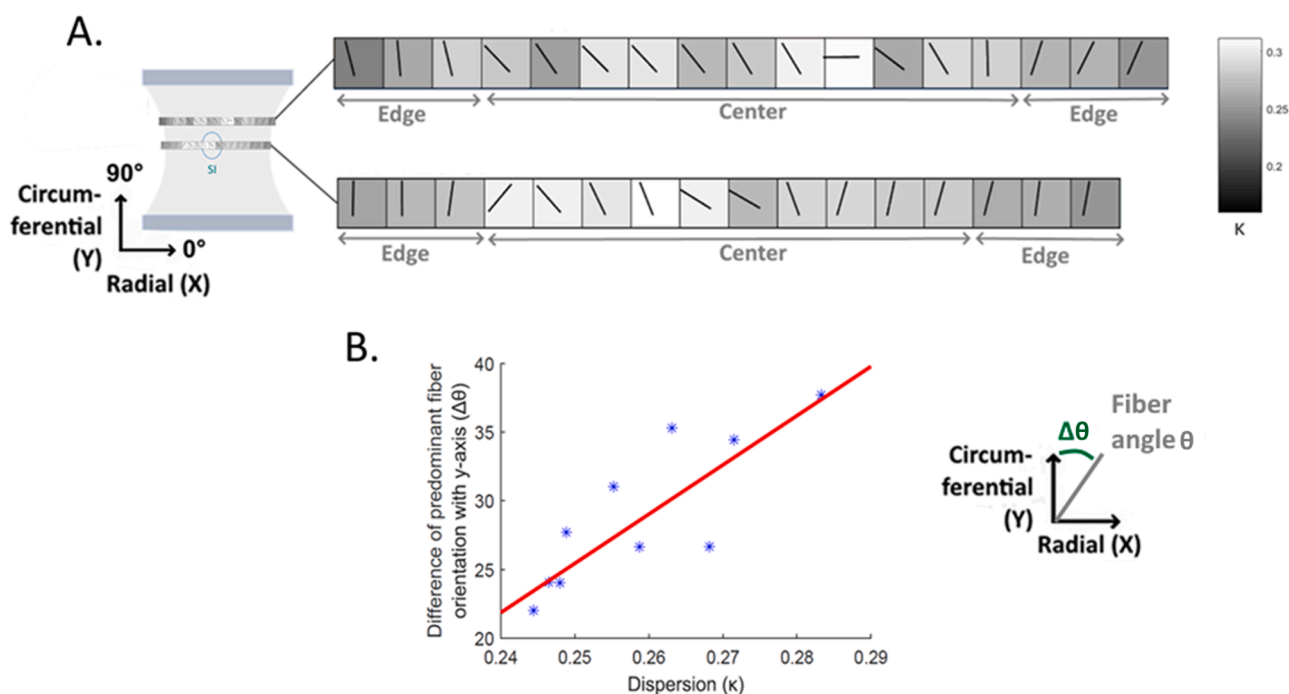


Fig. 2. A) The predominant orientation (black line) and dispersion,  $\kappa$ , (background color) of the fibers in the scanned regions of a cap analog, B) The correlation of the predominant fiber orientation and dispersion, both averaged per analog.

The average transversal cross-sectional area in the narrow mid-region of the mechanically tested analogs ( $n = 20$ ) was  $5.9 (\pm 0.8) \text{ mm}^2$ . Non-linear stiffening behavior was observed in the stress-strain curves. The median stiffness value was  $0.3 \text{ MPa}$  [Q1: Q3 =  $0.06:1.52$ ] at  $0.01$  strain and  $4.5 \text{ MPa}$  [ $1.8:8.9$ ] at  $0.07$  strain (the highest strain value before any rupture initiation in any of the samples). The median ultimate tensile stress was  $0.79 \text{ MPa}$  [ $0.55:1.05$ ] with an associated median strain value of  $0.15$  [ $0.13:0.18$ ].

Tangent stiffness at a strain of  $0.01$  correlated statistically significantly ( $p < 0.05$ ) with the fiber orientation ( $\theta$ ) and dispersion ( $\kappa$ ), showing higher stiffness with lower dispersion and better fiber alignment. However, the R-values indicated weak correlations (for  $\kappa$ :  $R = 0.74$  and for  $\theta$ :  $R = 0.74$ ). No significant correlation was found between tangent stiffness at a strain of  $0.07$  and these structural parameters.

### 3.3. Rupture initiation

In five analogs, the rupture started at a clamp whereas in the other fifteen analogs in the central region. Of the 15 analogs with central rupture, the rupture started in the SI in nine cases and at the SI-fibrous tissue interface in the other six cases. In Fig. 3A, the DIC-derived local tensile strain ( $\epsilon_{yy}$ ) measurements of a representative analog are shown at the frame right before the rupture initiation. Similar to this analog, all analogs ( $n = 20$ ) showed significantly higher tensile strain at the rupture site than the average strain within the analog (Median =  $1.21$  [Q1: Q3 =  $1.16:1.30$ ] vs  $1.14$  [ $1.12:1.17$ ],  $p < 0.001$ , Fig. 3B).

### 3.4. Rupture propagation

For the majority of the analogs, four rupture phases were identified (Fig. 4A): i.) a rupture starts in the SI, ii.) the rupture propagates within the SI towards the fibrous tissue-SI border, iii.) the rupture propagation pauses shortly ( $< 1$  second, 1–25 video frames) at the interface, iv.) then the rupture crosses the interface and propagates in the fibrous tissue, resulting in a rupture over the full width of the analog. In two analogs, a second rupture in the fibrous tissue was observed shortly after the first rupture started in the soft inclusion. These two ruptures propagated individually and eventually merged (Fig. 4B). As also illustrated in Fig. 4B, an analysis of rupture propagation direction and local predominant fiber direction revealed that the ruptures usually propagated parallel to the local fiber direction (Fig. 4C,  $R = 0.60$ ,  $\beta_1$  (slope of regression curve) =  $1.04$ ,  $p < 0.001$ ). The rupture propagation in the edge regions of the analogs was oriented closer to the y-direction than the rupture propagation in the center of the analogs (Fig. 4A, Bottom left).

The DIC-derived tensile strain ( $\epsilon_{yy}$ ) at the rupture site in the fibrous tissue, when the rupture propagated from the SI to the fibrous tissue, was significantly higher than the average strain within the fibrous tissue ( $0.21 \pm 0.05$  vs.  $0.16 \pm 0.04$ ,  $p < 0.05$ ). We further analyzed the fibrous tissue around the soft inclusion by dividing this region into 16 segments (Fig. 5A). It was noticed that  $\epsilon_{yy}$  in the fibrous tissue was highest on the sides of the SI (segments 15–16–1–2 and/or 7–8–9–10) and lowest above and/or below the SI (segments 3–4–5–6 and/or 11–12–13–14) (Fig. 5B). Rupture propagation that extended from the soft inclusion towards the fibrous tissue ( $n = 7$ ) consistently occurred on the sides of the SI (Fig. 5B).

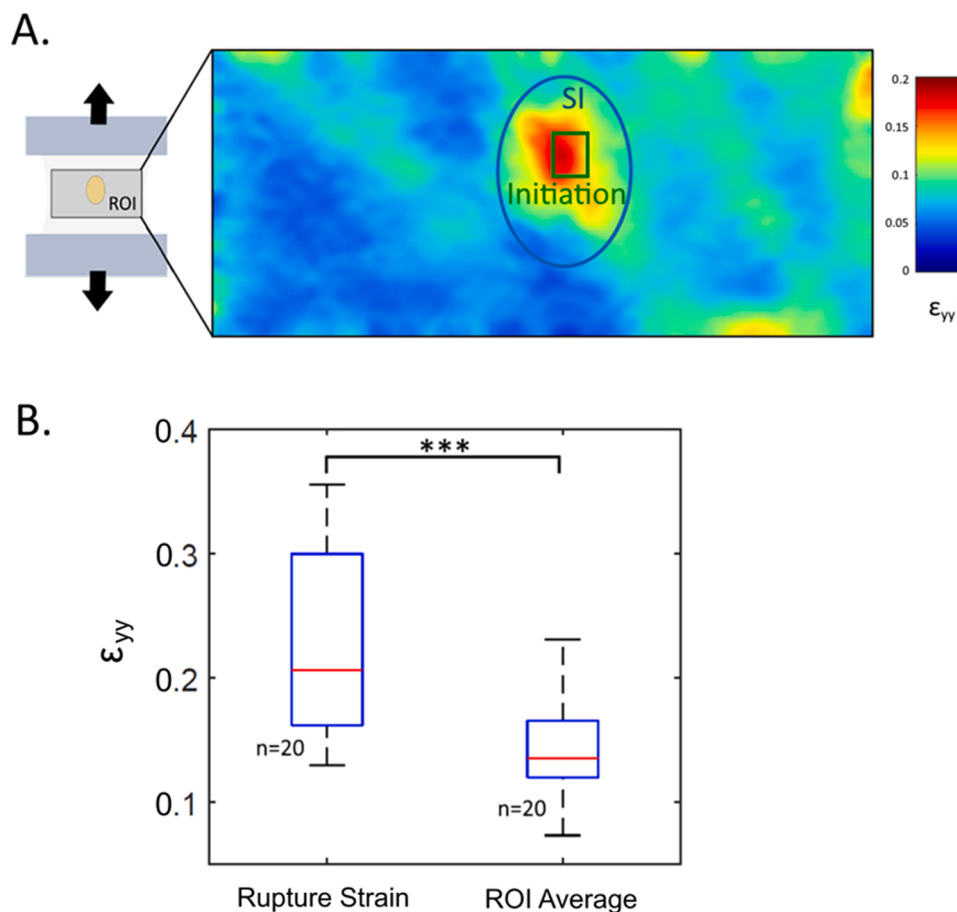


**Fig. 3.** A) DIC-derived tensile strain ( $\epsilon_{yy}$ ) distribution in a cap analog right before rupture initiation. The oval shape indicates the soft inclusion and the rectangle marks the rupture initiation region. B) Average tensile strain ( $\epsilon_{yy}$ ) in the rupture initiation region and in the ROI.

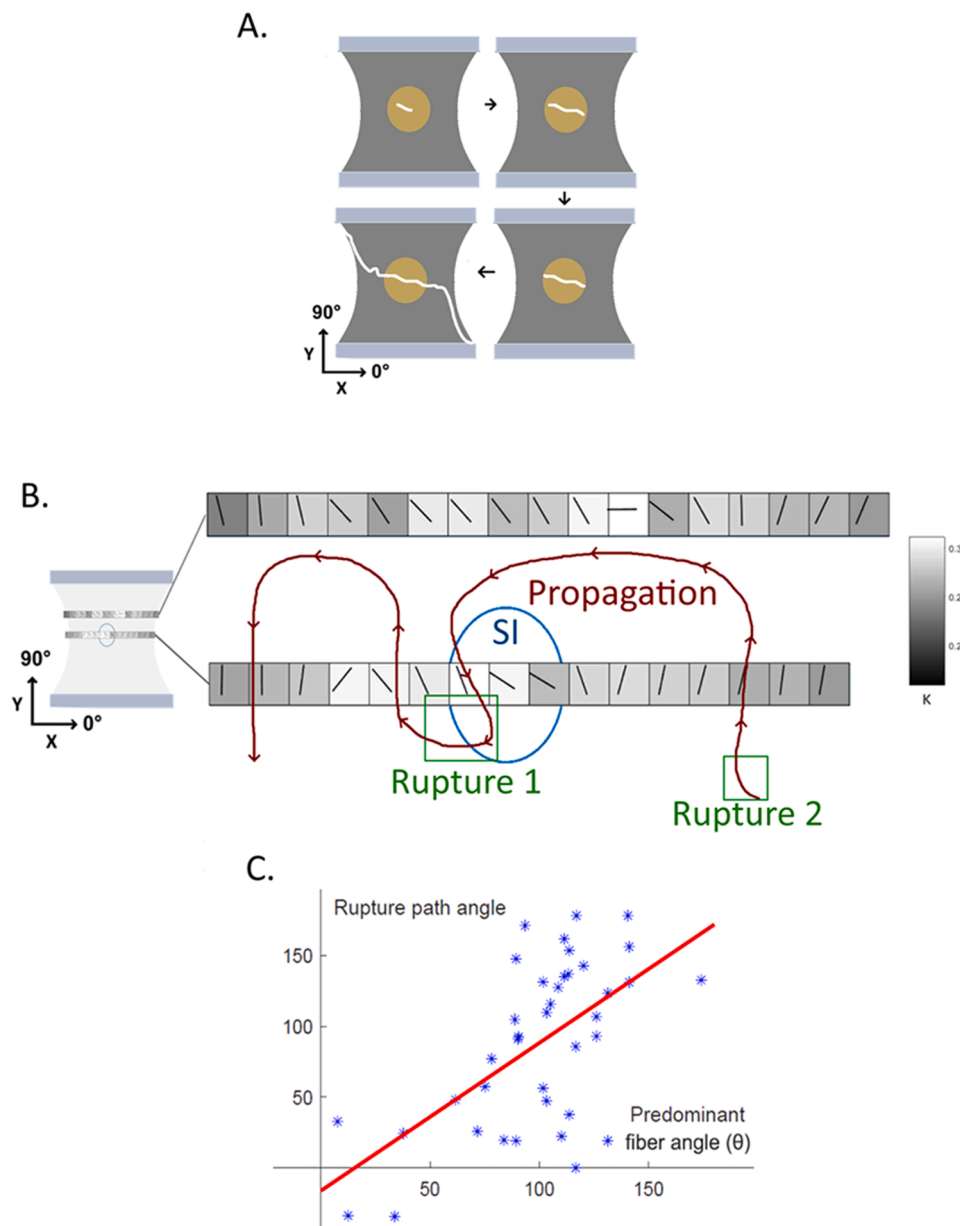


**Fig. 4.** Rupture propagation in the fibrous cap analogs A) Phases of rupture identified in cap analogs. Top left: Rupture initiation in SI, Top right: Rupture propagation within SI, Bottom right: Intermision, Bottom left: Fibrous tissue failure. B) Rupture path (red color) and fiber angle of one of the analogs. C) Fiber orientation vs. rupture path direction. Linear regression curve in red:  $R=0.60$ ,  $\beta_1$ (slope of regression curve) = 1.04,  $p < 0.001$ .

#### 4. Discussion

We investigated the (local) mechanical and structural properties of tissue-engineered fibrous cap analogs, a human disease model we recently developed [14] to understand the plaque rupture mechanics. We aimed to accomplish three key goals: (1) evaluate the analogs for their accuracy in mimicking the structural and mechanical properties of human fibrous cap tissue; (2) evaluate local strain for its usefulness as a marker for plaque rupture risk assessment and (3) identify correlations between structural and mechanical properties within our analogs that are challenging to observe in human tissue, but are crucial for enhancing our understanding and prediction of atherosclerotic plaque rupture. To meet these aims, we utilized uniaxial tensile testing coupled with DIC for acquiring mechanical behavior information and MPM-SHG imaging to gather the tissue's underlying collagen organization information.

The predominant fiber orientation analysis of the MIP images revealed that the majority of the fibers were oriented in the analogs' y-

direction, which corresponds to the circumferential direction in human plaques. In human plaques, the predominant fiber orientation varies among plaques and locally within a plaque [10,12], but in the majority of the plaques, the gross tissue fiber orientation is (close to) circumferential [11,12]. Thus, our results demonstrated that the created cap analogs mimic the dominant fiber direction of the human plaque caps. The fiber orientation analysis also demonstrated that there are local differences within analogs. In comparison to the center region, the edge regions of the analogs exhibited a more circumferential fiber orientation and less dispersion. This observed spatial variation in collagen organization, which is also present in real human plaques [10,11], allows us to investigate how the mechanics of the plaque are impacted by heterogeneity in fiber organization. The analysis of the MIP images revealed a correlation between the predominant fiber orientation and the degree of dispersion. Specifically, samples exhibiting lower dispersion demonstrated fibers that were oriented more towards the loading direction during culture. Foolen et al. previously demonstrated that increased

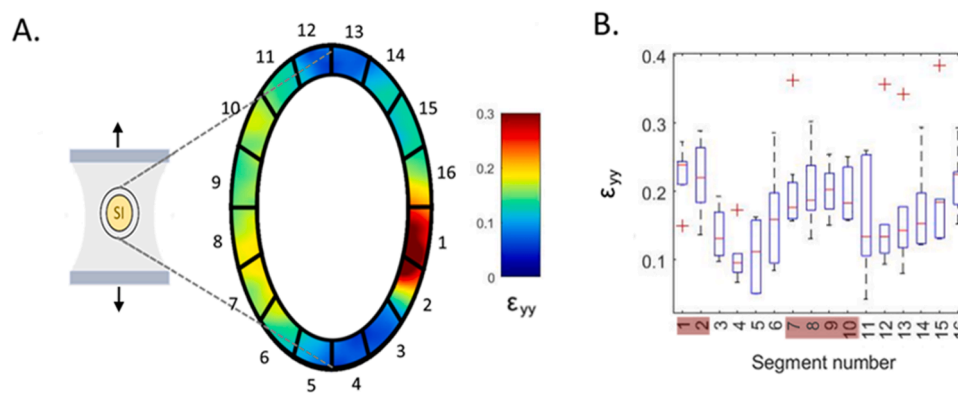


Fig. 5. A) Segmented DIC-derived local tensile strain ( $\epsilon_{yy}$ ) of a cap analog at the time point right before rupture propagation towards the fibrous tissue. B) DIC-derived local tensile strain ( $\epsilon_{yy}$ ) in the 16 segments of the analogs where the rupture propagated from the SI to the fibrous tissue ( $n=7$ ). The segments where rupture occurs in the analogs are marked red.

stretching in directions other than the loading direction during culture can promote greater dispersion and reduce the alignment of collagen in the loading direction through mechanotransduction mechanisms [22]. This effect can also contribute to the variation in dispersion and fiber angles observed among and within our tissue-engineered analogs. Specifically, we expect these variations to stem from differences in local stress and strain due to compaction during culturing, as well as geometric factors such as the precise location of the soft inclusion.

Uniaxial tensile tests revealed that all analogs demonstrated physiological strain stiffening responses with values that mimic plaque mechanical properties *ex vivo* [10,12]. The observed median stiffness values fall within the range of the values reported for human fibrous caps (0.1–5 MPa [23]). The analogs also showed global median ultimate strain values and global median ultimate stress values that fall within the range of the values reported for human fibrous caps and plaque tissue (0.04–0.23 and 0.1–2.0 MPa, respectively) [10,12]. Although within the typical range for human plaque tissue, the ultimate stress values are slightly higher and the ultimate strain values are lower in our analogs compared to the average values found in intact non-ulcerated human plaque tissue (0.6 MPa and 0.25) [24]. Numerical studies have suggested that the circumferential tensile stress experienced by the fibrous cap *in vivo* at the time of rupture is approximately 0.7 MPa [25], which is again quite similar to the stress we observed at rupture, though again slightly lower. These small discrepancies in mechanical properties might be due to the absence of macrophages and microcalcifications in our current model, since both increased macrophage and microcalcification density are known to increase strain and decrease maximum stress in plaque tissue [24,26,27]. Some of our future efforts will include integrating macrophages and microcalcifications [26] in the tissue-engineered analogs, to study their potential involvement in plaque rupture.

Tangent stiffness at low strain (0.01) showed a weak correlation with structural parameters, with higher stiffness linked to lower dispersion and greater circumferential fiber alignment ( $\theta$ ). However, this correlation was non-significant at a higher strain (0.07). We hypothesize that a correlation between tangent stiffness and structural parameters exists. However, since all our samples were cultured under similar conditions, variations in fiber angle and dispersion between samples were minimal. Consequently, the differences in stiffness in the current study may have been too small to detect. In another study, where we deliberately introduced different groups which increased the variation in dispersion, we observed a stronger correlation [26].

Daemen et al. previously reported fibrous cap fissures present along the interface between different plaque components (e.g., calcification-fibrous tissue) in human carotids [28]. This finding challenges the common expectation that the rupture initiates at the luminal side of the cap, and may imply that some cap ruptures originate in the deeper part

of the plaque. Our finding that all central ruptures in the tissue-engineered cap analogs initiated in the soft inclusion or at the interface between the soft inclusion and the fibrous tissue supports this hypothesis.

The analyses of the rupture path also revealed that the rupture propagation in the tissue-engineered analogs is commonly parallel to the local predominant fiber orientation. This phenomenon is particularly evident when comparing the rupture propagation paths at the analog edges to the ones in the analog centers. At the edges, both rupture propagation and collagen fibers were oriented in the tensile direction of the sample. In contrast, at the center of the sample, rupture propagation and collagen fibers exhibited an orientation more perpendicular to the loading direction. These findings suggest that in our analogs, the more dominant failure modes were matrix failure and/or fiber debonding, rather than fiber rupture. This is in line with the failure mode suggested by Daemen et al. for carotid plaque rupture [28]. Future studies with real plaques and/or tissue-engineered cap analogs are warranted for further confirmation of this hypothesis.

The DIC analysis revealed that regions of high strain were concentrated near the sites of rupture initiation and propagation in our cap analogs. These high-strain areas exhibited approximately 1.5 times greater strain values than the overall strain in the analogs. High-strain regions near the location of rupture initiation were also reported previously in human plaque tissue [10]. These findings highlight the critical need for local strain measurements to accurately characterize the failure behavior of fibrous plaque tissue. Moreover, these findings may suggest that local strain-based failure criteria may be useful for rupture risk prediction in atherosclerotic plaques, as also suggested earlier [29,30]. Unlike many other mechanical parameters, such as stress, strain can be assessed *in vivo* using imaging techniques like intravascular optical coherence tomography and ultrasound imaging [30,31]. To use the *in vivo* strain measurements for risk assessment, it would be beneficial to establish a cap rupture strain threshold. The rupture in the fibrous tissue is of particular interest, as it corresponds to cap rupture in real plaques. Conversely, rupture confined to the lipid pool (soft inclusion) poses no direct harm to the patient as long as it does not propagate in the fibrous tissue and reach the lumen. In our analogs, rupture initiation locations in the fibrous tissue (either originally started there or propagated from the SI to the fibrous tissue) had a median local strain value of 0.21. Strikingly, these strain values are similar to those at rupture locations of the fibrous tissue of real plaques, reported to be  $>0.10$  with a median value of 0.25 [10]. Note that the CAE specimens from this study [10] were harvested from regions of the carotid artery which might be beyond the atheroma; in this case, the distribution of collagen fibres and mechanical properties would differ from the fibrous cap of the atheroma. Unfortunately, this is currently the only available literature examining local plaque mechanics and local fiber orientation, making it the only viable

comparison. Moreover, our DIC analysis revealed that while rupture initiation and propagation consistently occurred in high-strain regions, these were not always the only areas with the highest strain. These multiple high-strain regions within the same sample make establishing an exact strain threshold for rupture risk challenging. Therefore, while strain can be a valuable marker for assessing rupture risk, it may need to be supplemented with other mechanical or structural markers for a more reliable and comprehensive evaluation.

There are some limitations associated with this study. (1) Consistent with previous studies [14,26], the analogs demonstrated a nonuniform collagen structure along the depth direction. The upper section of the analogs exhibited a higher intensity SHG signal, which suggests greater collagen density, and a more pronounced predominant fiber orientation, possibly due to increased nutrient availability at the surface. Due to this higher collagen density and more pronounced fiber orientation this upper layer is expected to dominate the overall stiffness and strength of the analogs. We anticipate that the findings on the relationship between structural and mechanical behavior remain valid, as also structural measurements are likely dominated by the upper layer. (2) The human plaques are under a multiaxial loading state *in vivo*, which is more complex than the uniaxial tensile loading applied to the cap analogs in the current study. Atherosclerotic plaques are subjected to two main types of loading: blood pressure and shear forces caused by blood flow. However, the shear stresses are much smaller—approximately three orders of magnitude—compared to the stresses induced by blood pressure [32]. As a result, the mechanical role of shear forces in cap rupture is negligible, and rupture is primarily attributed to the stresses caused by blood pressure. Consequently, tensile tests were conducted in the circumferential direction, as this is the dominant loading direction *in vivo* due to the circumferential stresses induced by blood pressure. (3) Another limitation of our study is the homogeneity of the tissue-engineered cap analogs. While this homogeneity facilitates the relatively easy establishment of relationships between structural parameters and mechanical properties, it may not fully capture the structural heterogeneity observed in some human plaques. Nevertheless, the flexibility of our analogs provides control over various structural parameters, making them a valuable platform for future research. In subsequent studies, we plan to introduce greater heterogeneity into our analogs to more closely mimic the complex variations in human plaques. These variations will be added incrementally to investigate the impact of each individual compound or modification, allowing us to explore how such variability affects plaque mechanics. Although these enhancements were not part of the current study, which focused on validating the basic model, we can modify several key structural parameters in future work. For example, we could adjust the inclusion of calcification mimics [26] or alter the collagen structure by introducing compounds like TGF- $\beta$ , ribose, copper, or beta-aminopropionitrile during culture. These modifications could stimulate collagen deposition, promote advanced glycation end-product (AGE)-related crosslinking, and modulate lysyl oxidase (LOX)-mediated crosslinking.

## 5. Conclusion

In this study, we evaluated in detail the mechanical and structural characteristics of tissue-engineered atherosclerotic cap analogs, which we developed recently as a human disease model to understand atherosclerotic plaque rupture. Our findings demonstrated a good resemblance of the analogs with real plaque fibrous caps, both for collagen architecture and mechanical behavior. Furthermore, our analogs provided further insight into plaque rupture, by demonstrating local strain concentrations at the rupture sites and the influence of local collagen fiber architecture on rupture propagation direction, where the former suggests a potential use of *in vivo* local strain measurements for plaque rupture risk assessment.

## Funding statement

This work was supported by an NWO-Vidi grant [18360]; and the European Research Council (ERC) under Horizon 2020 research and innovation program [101042724 — MicroMechAthero].

## CRedit authorship contribution statement

**Hanneke Crielaard:** Writing – review & editing, Writing – original draft, Project administration, Methodology, Investigation, Formal analysis, Data curation, Conceptualization. **Tamar B. Wissing:** Writing – review & editing, Methodology, Investigation, Conceptualization. **Su Guvenir Torun:** Writing – review & editing, Investigation. **Gert-Jan Kremers:** Writing – review & editing, Methodology. **Pablo de Miguel:** Writing – review & editing, Methodology, Investigation. **Ranmadusha M. Hengst:** Writing – review & editing, Methodology, Investigation. **Frank J.H. Gijzen:** Writing – review & editing, Supervision, Conceptualization. **Ali C. Akyildiz:** Writing – review & editing, Supervision, Conceptualization. **Kim van der Heiden:** Writing – review & editing, Supervision, Conceptualization.

## Declaration of competing interest

The authors declare that they have no known competing financial interests or personal relationships that could have appeared to influence the work reported in this paper.

## Supplementary materials

Supplementary material associated with this article can be found, in the online version, at doi:10.1016/j.actbio.2025.01.035.

## References

- [1] P. Libby, J.E. Buring, L. Badimon, G.K. Hansson, J. Deanfield, M.S. Bittencourt, L. Tokgozöglu, E.F. Lewis, Atherosclerosis, Nat. Rev. Dis. Primers. 5 (2019) 1–18, <https://doi.org/10.1038/s41572-019-0106-z>.
- [2] F. Visseren, F. Mach, Y.M. Smulders, D. Carballo, K.C. Koskinas, M. Böck, A. Benetos, A. Biffi, J.M. Boavida, D. Capodanno, B. Cosyns, C.A. Crawford, C. H. Davos, I. Desormais, E. Di Angelantonio, O.H.F. Duran, S. Halvorsen, F. D. Richard Hobbs, M. Hollander, E.A. Jankowska, M. Michal, S. Sacco, N. Sattar, L. Tokgozöglu, S. Tonstad, K.P. Tsoufis, I. van Dis, I.C. van Gelder, C. Wanner, B. Williams, G. De Backer, V. Regitz-Zagrosek, A.H. Aamodt, M. Abdelhamid, V. Aboyans, C. Albus, R. Asteggiano, M. Böck, M.A. Borger, C. Brotons, J. Celutkiene, R. Cifkova, M. Cikes, F. Cosentino, N. Dagres, T. De Backer, D. De Bacquer, V. Delgado, H. Den Ruijter, P. Dendale, H. Drexel, V. Falk, L. Fauchier, B. A. Ference, J. Ferrières, M. Ferrini, M. Fisher, D. Fliser, Z. Fras, D. Gaita, S. Giampaoli, S. Gielen, I. Graham, C. Jennings, T. Jorgensen, A. Kautzky-Willer, M. Kavousi, W. Koenig, A. Konradi, D. Kotecha, U. Landmesser, M. Lettino, B. S. Lewis, A. Linhart, M.L. Løchen, K. Makrillakis, G. Mancía, P. Marques-Vidal, J. W. McEvoy, P. McGreevy, B. Merkely, L. Neubeck, J.C. Nielsen, J. Perk, S. E. Petersen, A.S. Petronio, M. Piepoli, N.G. Pogosova, E.I.B. Prescott, K.K. Ray, Z. Reiner, D.J. Richter, L. Rydén, E. Shlyakhto, M. Sitges, M. Sousa-Uva, I. Sudano, M. Tiberi, R.M. Touyz, A. Ungar, W.M. Monique Verschuren, O. Wiklund, D. Wood, J.L. Zamorano, 2021 ESC guidelines on cardiovascular disease prevention in clinical practice, Eur. Heart. J. 42 (2021) 3227–3337, <https://doi.org/10.1093/eurheartj/ehab484>.
- [3] I.K. Jang, G.J. Tearney, B. MacNeill, M. Takano, F. Moselewski, N. Iftima, M. Shishkov, S. Houser, H.T. Aretz, E.F. Halpern, B.E. Bouma, *In vivo* characterization of coronary atherosclerotic plaque by use of optical coherence tomography, Circulation 111 (2005) 1551–1555, <https://doi.org/10.1161/01.CIR.0000159354.43778.69>.
- [4] J. Ohayon, G. Finet, A.M. Gharib, D.A. Herzka, P. Tracqui, J. Heroux, G. Rioufol, M. S. Kotys, A. Elagha, R.I. Pettigrew, Necrotic core thickness and positive arterial remodeling index: emergent biomechanical factors for evaluating the risk of plaque rupture, Am. J. Physiol. Heart. Circ. Physiol. 295 (2008) H717–H727, <https://doi.org/10.1152/ajpheart.00005.2008>.
- [5] SCOT-HEART Investigators, Coronary CT angiography and 5-year risk of myocardial infarction, New England J. Med. 379 (2018) 924–933, <https://doi.org/10.1056/NEJMoa1805971>.
- [6] M.C. Williams, A.J. Moss, M. Dweck, P.D. Adamson, S. Alam, A. Hunter, A.S. V. Shah, T. Pawade, J.R. Weir-McCall, G. Roditi, E.J.R. van Beek, D.E. Newby, E. D. Nicol, Coronary artery plaque characteristics associated with adverse outcomes in the SCOT-HEART study, J. Am. Coll. Cardiol. 73 (2019) 291–301, <https://doi.org/10.1016/j.jacc.2018.10.066>.

- [7] B.R. Kwak, M. Bäck, M.L. Bochaton-Piallat, G. Caligiuri, M.J.A.P. Daemen, P. F. Davies, I.E. Hofer, P. Holvoet, H. Jo, R. Krams, S. Lehoux, C. Monaco, S. Steffens, R. Virmani, C. Weber, J.J. Wentzel, P.C. Evans, Biomechanical factors in atherosclerosis: mechanisms and clinical implications, *Eur. Heart J.* 35 (2014) 3013–3020, <https://doi.org/10.1093/eurheartj/ehu353>, 3020a–3020d.
- [8] G.A. Holzapfel, Collagen in arterial walls: biomechanical aspects, in: *Collagen*, Springer US, Boston, MA, n.d.: pp. 285–324. [https://doi.org/10.1007/978-0-387-73906-9\\_11](https://doi.org/10.1007/978-0-387-73906-9_11).
- [9] M. Rekhter, Collagen synthesis in atherosclerosis: too much and not enough, *Cardiovasc. Res.* 41 (1999) 376–384, [https://doi.org/10.1016/S0008-6363\(98\)00321-6](https://doi.org/10.1016/S0008-6363(98)00321-6).
- [10] S.G. Torun, P.D.M. Munoz, H. Crielaard, H.J.M. Verhagen, G.J. Kremers, A.F. W. van der Steen, A.C. Akyildiz, Local characterization of collagen architecture and mechanical failure properties of fibrous plaque tissue of atherosclerotic human carotid arteries, *Acta Biomater.* 164 (2023), <https://doi.org/10.1016/j.actbio.2023.04.022>.
- [11] A.C. Akyildiz, C.K. Chai, C.W.J. Oomens, A. van der Lugt, F.P.T. Baaijens, G. J. Strijkers, F.J.H. Gijzen, 3D Fiber orientation in atherosclerotic carotid plaques, *J. Struct. Biol.* 200 (2017) 28–35, <https://doi.org/10.1016/j.jsb.2017.08.003>.
- [12] R.D. Johnston, R.T. Gaul, C. Lally, An investigation into the critical role of fibre orientation in the ultimate tensile strength and stiffness of human carotid plaque caps, *Acta Biomater.* 124 (2021) 291–300, <https://doi.org/10.1016/j.actbio.2021.02.008>.
- [13] H. Crielaard, S.G. Torun, T.B. Wissing, P.M. Muñoz, G.J. Kremers, F.J.H. Gijzen, K. Van Der Heiden, A.C. Akyildiz, A method to study the correlation between local collagen structure and mechanical properties of atherosclerotic plaque fibrous tissue, *J. Visualiz. Exper.* 2022 (2022), <https://doi.org/10.3791/64334>.
- [14] T.B. Wissing, K. Van Der Heiden, S.M. Serra, A.I.P.M. Smits, C.V.C. Bouten, F.J.H. Gijzen, Tissue-engineered collagenous fibrous cap models to systematically elucidate atherosclerotic plaque rupture, (n.d.). <https://doi.org/10.1101/2021.07.20.451997>.
- [15] M.P. Rubbens, A. Mol, R.A. Boerboom, R.A. Bank, F.P.T. Baaijens, C.V.C. Bouten, Intermittent straining accelerates the development of tissue properties in engineered heart valve tissue, *Tissue Eng. Part A* 15 (2009) 999–1008, <https://doi.org/10.1089/ten.tea.2007.0396>.
- [16] A.F. Frangi, K.L. Vincken, W.J. Niessen, M.A. Viergever, Multiscale vessel enhancement filtering computational cardiac image analysis view project FocusDET view project Multiscale vessel enhancement filtering, n.d. <https://www.researchgate.net/publication/2388170>.
- [17] J. Blaber, B. Adair, A. Antoniou, Ncorr: open-source 2D digital image correlation matlab software, *Exp. Mech.* 55 (2015) 1105–1122, <https://doi.org/10.1007/s11340-015-0009-1>.
- [18] M.T. Walsh, E.M. Cunnane, J.J. Mulvihill, A.C. Akyildiz, F.J.H. Gijzen, G. A. Holzapfel, Uniaxial tensile testing approaches for characterisation of atherosclerotic plaques, *J. Biomech.* 47 (2014) 793–804, <https://doi.org/10.1016/j.jbiomech.2014.01.017>.
- [19] J.D. Humphrey, S.L. Delange, *An Introduction to Biomechanics*, Springer New York, New York, NY, 2004, <https://doi.org/10.1007/978-1-4899-0325-9>.
- [20] R.A. Macrae, K. Miller, B.J. Doyle, Methods in mechanical testing of arterial tissue: A review, *Strain.* 52 (2016) 380–399, <https://doi.org/10.1111/str.12183>.
- [21] J. Schindelin, I. Arganda-Carreras, E. Frise, V. Kaynig, M. Longair, T. Pietzsch, S. Preibisch, C. Rueden, S. Saalfeld, B. Schmid, J.Y. Tinevez, D.J. White, V. Hartenstein, K. Eliceiri, P. Tomancak, A. Cardona, Fiji: an open-source platform for biological-image analysis, *Nat. Methods* 9 (2012) 676–682, <https://doi.org/10.1038/nmeth.2019>.
- [22] J. Foolen, V.S. Deshpande, F.M.W. Kanters, F.P.T. Baaijens, The influence of matrix integrity on stress-fiber remodeling in 3D, *Biomaterials* 33 (2012) 7508–7518, <https://doi.org/10.1016/j.biomaterials.2012.06.103>.
- [23] A.C. Akyildiz, L. Speelman, F.J.H. Gijzen, Mechanical properties of human atherosclerotic intima tissue, *J. Biomech.* 47 (2014) 773–783, <https://doi.org/10.1016/j.jbiomech.2014.01.019>.
- [24] C.L. Lendon, M.J. Davies, G.V.R. Born, P.D. Richardson, Atherosclerotic plaque caps are locally weakened when macrophages density is increased, *Atherosclerosis* 87 (1991) 87–90, [https://doi.org/10.1016/0021-9150\(91\)90235-U](https://doi.org/10.1016/0021-9150(91)90235-U).
- [25] Z.Y. Li, S. Howarth, R.A. Trivedi, J.M. U-King-Im, M.J. Graves, A. Brown, L. Wang, J.H. Gillard, Stress analysis of carotid plaque rupture based on *in vivo* high resolution MRI, *J. Biomech.* 39 (2006) 2611–2622, <https://doi.org/10.1016/j.jbiomech.2005.08.022>.
- [26] I. Jansen, H. Crielaard, T. Wissing, C. Bouten, F. Gijzen, A.C. Akyildiz, E. Farrell, K. van der Heiden, A tissue-engineered model of the atherosclerotic plaque cap: toward understanding the role of microcalcifications in plaque rupture, *APL Bioeng.* 7 (2023), <https://doi.org/10.1063/5.0168087>.
- [27] I. Jansen, R. Cahalane, R. Hengst, A. Akyildiz, E. Farrell, F. Gijzen, E. Aikawa, K. van der Heiden, T. Wissing, The interplay of collagen, macrophages, and microcalcification in atherosclerotic plaque cap rupture mechanics, *Basic Res. Cardiol.* 119 (2024) 193–213, <https://doi.org/10.1007/s00395-024-01033-5>.
- [28] M.J. Daemen, M.S. Ferguson, F.J. Gijzen, D.S. Hippe, M.E. Kooi, K. Demarco, A. C. van der Wal, C. Yuan, T.S. Hatsukami, Carotid plaque fissure: an underestimated source of intraplaque hemorrhage, *Atherosclerosis* 254 (2016) 102–108, <https://doi.org/10.1016/j.atherosclerosis.2016.09.069>.
- [29] O. Lisický, A. Hrubanová, R. Staffa, R. Vlachovský, J. Burša, Constitutive models and failure properties of fibrous tissues of carotid artery atheroma based on their uniaxial testing, *J. Biomech.* 129 (2021) 110861, <https://doi.org/10.1016/j.jbiomech.2021.110861>.
- [30] J.A. Schaar, C.L. De Korte, F. Mastik, C. Strijder, G. Pasterkamp, E. Boersma, P. W. Serruys, A.F.W. Van Der Steen, Characterizing vulnerable plaque features with intravascular elastography, *Circulation* 108 (2003) 2636–2641, <https://doi.org/10.1161/01.CIR.0000097067.96619.1F>.
- [31] T. Wang, T. Pfeiffer, A. Akyildiz, H.M.M. van Beusekom, R. Huber, A.F.W. van der Steen, G. van Soest, Intravascular optical coherence elastography, *Biomed. Opt. Express.* 13 (2022) 5418–5433, <https://doi.org/10.1364/BOE.470039>.
- [32] P.R. Hoskins, D. Hardman, Three-dimensional imaging and computational modelling for estimation of wall stresses in arteries, *Br. J. Radiol.* 82 (2009) S3–S17, <https://doi.org/10.1259/bjr/96847348>.